minimum value. This configuration leads to an upper bound for the coefficient of variation of $(x_M - x_m)(n-1)^{1/2}/[x_M + (n-1)x_m]$.

The aforementioned upper bound, however, is inappropriate for the case at hand, since the distribution that led to it is specifically prohibited on the basis of assumption 2. The worst possible distribution that does not contradict assumption 2 corresponds to one where x_m is zero and where half the terms are equal to x_m and the rest to x_M. This leads to a coefficient of variation of unity, thus establishing an upper bound compatible with the assumptions of the proposed method.

To illustrate the tendency for V to satisfy the constraints previously established, i.e., $0 \leq V \leq 1$, we refer to Table 1 where V varied only from 0.333 to 0.764 for the wide variety of one-sided distributions considered.

References

[1] Cramer, H., *Mathematical Methods of Statistics*, Princeton Univ. Press, Princeton, New Jersey, 1958.

[2] Bellman, R., *Adaptive Control Processes, A Guided Tour*, Princeton Univ. Press, Princeton, N. J., 1961.

Arc Motion in High-Pressure Cross-Field Devices

R. B. Stewart* and A. P. Sabol†
NASA Langley Research Center, Hampton, Va.

RECENT experiments by the authors with several coaxial cross-field plasma devices have shown some anomalous behavior in the rotational speeds of an arc. Because of the present interest in such devices, pertinent aspects of the experiments are summarized and one explanation is proposed for the observed phenomena.

Three concentric, cross-field configurations designated as "A," "B," and "A"$_{mod}$ are considered. Device "A" is shown schematically in Fig. 1a. It provides for heating and acceleration of the gas within a vortex chamber and is being developed for use with hypervelocity wind tunnels, see Refs. 1 and 2. The "A" devices operate from a direct current power supply with an externally applied magnetic field. Figure 1b is a schematic of the "B" devices. Experiments made with these devices are reported in Ref. 3. Although these latter tests were of a pulsed nature, the current flow as well as the rotational speed of the arc reached steady values before the circuit was interrupted. Two principle differences exist between the "A" and "B" devices. In "A" the cathode surface is a logarithmic spiral of the form $r = ae^{m\Theta}$ and as such provides for a radially outward displacment of the cathode surface. The second difference is the impressed gas flow arrangement. All of the experiments with the "A" devices were made with a mass flow of gas forced radially outward across the vortex. In the "B" devices, no such flow was impressed on the vortex, but gradients established by the vortex were solely responsible for any flow of gas. Figure 1c schematically shows the third device, which is an "A" device modified with a circular cylindrical cathode geometry. In all three devices the motion of the arc was observed by means of light pipes connected to oscilloscopes through emitter follwers circuits.

Figure 2 shows the measured cathode root velocities as a function of the electromagnetic driving parameter BI. The arc current ranged from 1300 amp to 4600 amp. The chamber pressure levels and magnetic field strength are indicated for each set of data. The cathode root velocities for the "A" devices are seen to be anomalously high compared with the velocities measured in the "B" devices. The electrode gap in the "B" devices was changed from 1.27 cm to 2.54 cm with almost no effect on the cathode root velocities. Also, the effect of an impressed radial mass flow was investigated in the "A"$_{mod}$ device by tests made with and without endwalls and with and without a forced mass flow. Little effect was found from these changes, as can be seen in Fig. 2. The conclusion that radial mass flow does not have a significant effect on the vortex would be erroneous, however, because even with no endwalls the vortex establishes a substantial outward radial flow with gas being discharged near the cathode surface. This fact was observed during tests with the endwalls removed. For the tests at the highest current and applied magnetic field strengths, the cathode root velocity in the spiral cathode arrangement is more than four times greater than the root velocity for the circular cathode.

Probable Cause of Anomalous Cathode Root Velocities

Electromagnetic effects offer one explanation for the high cathode root velocities in the spiral geometries. Figure 3 illustrates a simple model of a spiral geometry and shows how the cathode sheath moves radially outward across lines of applied magnetic flux during each rotation of the arc column. Since high ion densities occur near the surface of metal cathodes, the outward radial motion of this sheath constitutes a noticeable "local" current that provides a Lorentz force in

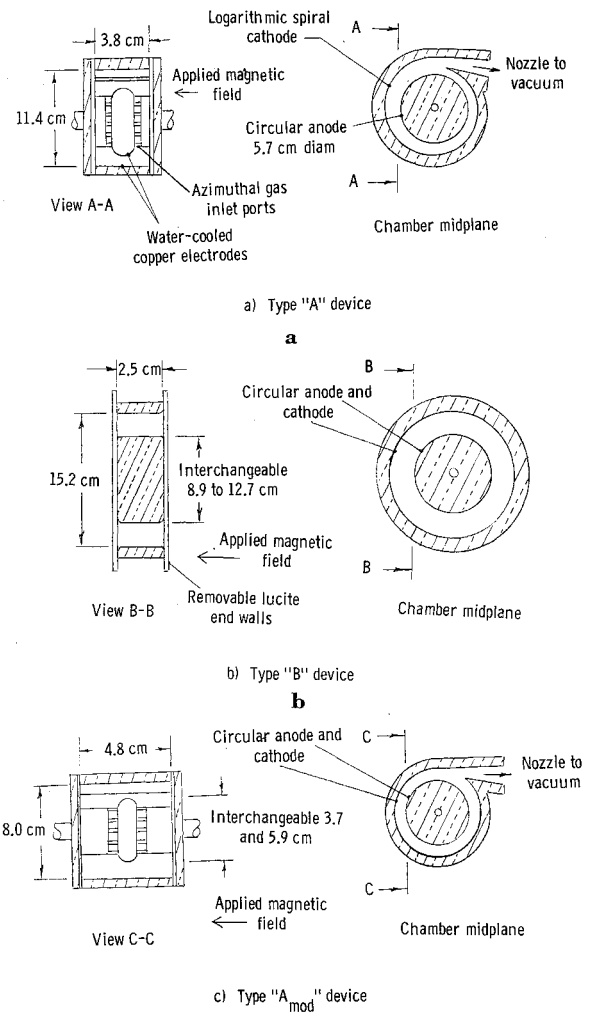

Fig. 1 Experimental crossed field devices.

Received March 21, 1969; revision received June 6, 1969.

* Aero-Space Technologist, High Temperature Fluid Mechanics Section, Aero-Physics Division. Member AIAA.

† Aero-Space Technologist, High Temperature Fluid Mechanics Section, Aero-Physics Division.

addition to the Lorentz force due to electron and ion current conduction within the arc column. This local force is present in such devices, as shown in Fig. 1a whenever the cathode surface diverges outward. From Fig. 3, the radial displacement of the cathode sheath is:

$$\text{Displacement} = \int_0^\Theta ame^{m\Theta}d\Theta, \text{ cm} \qquad (1)$$

The local current is given by the rate at which ions in the sheath are moved through this displacement distance. Periodic radial motion of the arc and cathode sheath is established by rotation of the arc within the spiral geometry. The additional azimuthal Lorentz force is the vector cross product of the local radial current and the applied axial magnetic field. A mathematical formulation that includes both the column and sheath forces is complicated and requires matching of solutions at each boundary under time dependent conditions. Such a solution is not attempted here; however, an order of magnitude analysis illustrates the possible increase in the resulting electromagnetic driving force. The assumption is made that the spiral geometry and the nonequilibrium effects in the arc column do not alter the electron motion or number density in the sheath, nor do they alter the over-all arc motion or the ion density in the sheath. With these considerations the local ion current density can be written as:

$$J^+_{\text{local}} = n_i e\dot{r}, \text{ amp/cm}^2 \qquad (2)$$

where n_i = ion density per unit volume in the cathode sheath, e = electronic charge per ion, and $\dot{r}$ = radial velocity of sheath. With regard to the ion density in the sheath, a value of 10^{19} ions/cm^3 is taken as a conservative estimate considering the high ion current densities (on the order of 10^5 amp/cm^2) that have been observed on metal electrodes. There is evidence that for low boiling point metal cathodes the value of n_i approaches the density of the electrode material.[4] For copper this value is 8×10^{22} atoms/cm^3. In any event, values of n_i of 10^{19} or greater will produce a singificant local Lorentz force on the sheath. From Ref. 4, the ion conduction current is taken as 0.1 of the current due to electron conduction. For the range of the present experiments this gives a cathode spot area of $0(10^{-3}$ cm$^2)$.

The radial sheath velocity is obtained from the measured rotational period of the highest observed cathode root velocity in the "A" devices. This value is 3×10^{-5} sec. Using these values and a displacement of 1.5 cm Eq. (2) gives an order of magnitude result for the local current;

$$J^+_{\text{local}} = \frac{10^{19}\,1.6 \times 10^{-19}\,1.5}{3 \times 10^{-5}} = 8 \times 10^4 \frac{\text{amp}}{\text{cm}^2} \qquad (3)$$

This local current density is of the same order as the current density due to ion current conduction on metal cathodes, and can produce a significant additional Lorentz force on the sheath. This force is in the same azimuthal direction as that caused by the conduction current.

The proposed explanation suggests that displacement of the cathode sheath in spiral electrode geometries produces markedly higher arc rotational speeds than in the circular geometries. As shown in Fig. 2, this increase in speed is appreciable. Figure 4 shows, in a normalized form, that at low velocities the gain in speed in the spiral geometry is three times greater than that with the circular geometry for only twice the input of energy. However, at the higher velocities, significantly higher input energy is required. This might be expected because of friction losses. These results show that up to six times the input power is required for a gain in velocity of about four times that of the circular geometry. The results of Fig. 4 are presented as the ratio of velocities per unit Lorentz force, a form that eliminates a dependence on the magnetic driving force, and as the ratio of gas enthalpies to eliminate any effects due to differences in gas flow rates. Gas enthalpies were determined by establishing a heat balance between the measured input and output quantities while the devices operated at a steady-state weight flow.

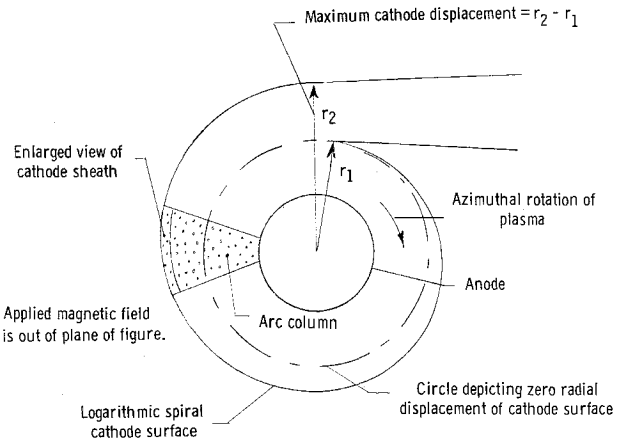

Fig. 3 Spiral geometry for cathode and cathode sheath displacement.

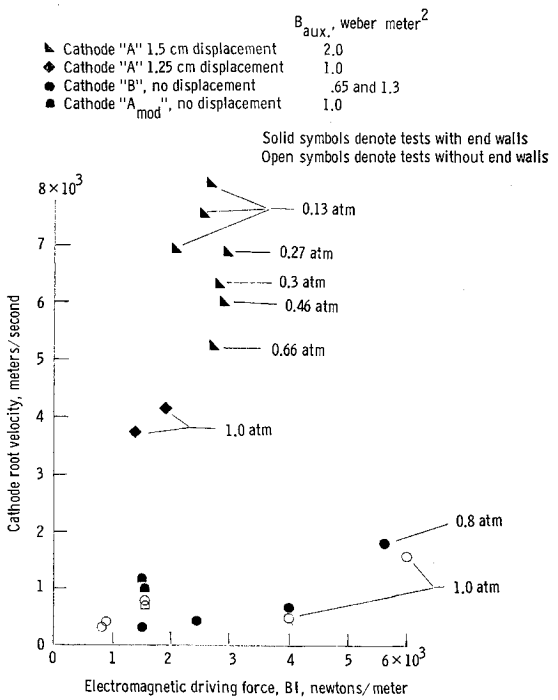

Fig. 2 Experimental cathode root velocities.

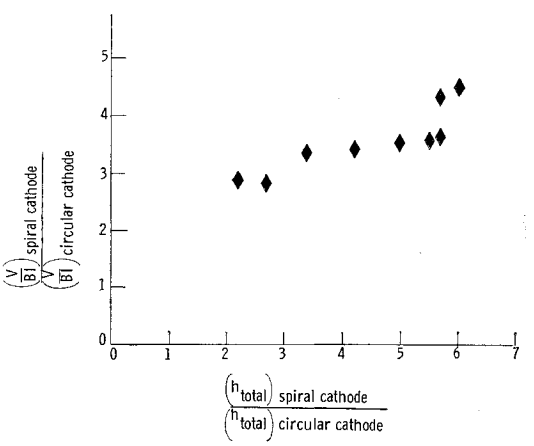

Fig. 4 Experimental velocity vs total gas energy.

References

[1] Stewart, R. B. and Wallio, M. A., "The Experimental Performance of an Arc Driven Vortex Type Heater Accelerator," *Proceedings of the Fourth Hypersonic Technology Symposium*, Tullahoma, Tenn., 1965, pp. 172–206.

[2] Stewart, R. B., "An Analysis of an Electromagnetically Driven Confined Vortex with High Positive Radial Reynolds Numbers," AIAA Paper 67-730, Colorado Springs, Colo., 1967.

[3] Sabol, A. P., Stewart, R. B., and Duckett, R. J., "An Experimental Study of the Behavior of High Current Arcs Driven by Strong External Magnetic Fields," *Proceedings of the Eighth Symposium on Engineering Aspects of MHD*, March 1967, pp. 130–131.

[4] Finkelnburg, W. and Maecker, H., "Electrische Bogen und Thermisches Plasma," *Encyclopedia of Physics*, transl., Vol. XXII, Gas Discharges II, Springer-Verlag, 1956.

Effect of Angle-of-Attack Oscillation on the Stability of Liquid Films

Ali Hasan Nayfeh*

Aerotherm Corporation, Mountain View, Calif.

Introduction

To derive the maximum benefit of a melting ablator, or a transpiration coolant on a re-entry body, the liquid layer should remain in contact with the re-entry body, and its removal should be in the form of vapor only. There are a number of instability mechanisms that may lead to the loss of the liquid layer before deriving the benefit of its vaporization, depending on the position of the liquid layer on the body. Away from the stagnation region, the Kelvin-Helmholtz[1] and Craik-Benjamin[2] instability mechanisms, among others, may be important. In the stagnation region, the Lamb-Taylor mechanism[3,4] is important because it is characterized by high deceleration forces acting outwards from the liquid layer. At zero angle of attack, the liquid has little relative motion, and the deceleration force has no oscillations. At angle of attack, the pressure at the windward side is higher than that at the leeward side, and hence relative motion of the liquid exists in the stagnation region due to the pressure gradient. Moreover, an oscillatory component of deceleration is produced due to angle-of-attack oscillations. The purpose of this Note is to show that this oscillatory component of deceleration is destabilizing.

Before proceeding with the analysis, let us discuss some of the pertinent work on the Lamb-Taylor instability mechanism. Lamb[3] and then Taylor[4] showed that, in the absence of surface tension and viscosity, a liquid layer in an acceleration field directed outwards from the liquid, is inherently unstable for disturbances of all wave lengths. Bellman and Pennington[5] showed that surface tension stabilizes wave numbers above the cutoff wave number $k_c = (\rho g/T)^{1/2}$, where g is the acceleration normal to the liquid surface, and ρ and T are the liquid density and surface tension, respectively. They also showed that viscosity reduces the amplification rate, but could never by itself make it go to zero for any finite wave length.

Although the analysis of Ref. 5 shows that disturbances with wave numbers greater than k_c are fully stabilized by surface tension (i.e., only oscillatory motion with time-independent amplitude is possible), Emmons, Chang and Watson[6] observed experimentally that these waves oscillated with an ever increasing amplitude. The acceleration was provided in their experiment by stretched rubber bands. They attempted to explain this instability using nonlinear analysis. However, Nayfeh[7] pointed out that their analysis is valid only for short times and cannot be used to explain this behavior that was observed beyond the validity of the expansion. Nayfeh also showed that the nonlinearity modifies the cutoff wave number to

$$\tilde{k}_c = k_c\,[1 + \tfrac{3}{8}\eta_0^2 k_c^2 + \tfrac{51}{512}\eta_0^4 k_c^4]^{1/2} \tag{1}$$

with η_0 the initial amplitude. Above this wave number disturbances oscillate with time-independent amplitudes though with amplitude-dependent frequencies. Hence, he pointed out that the physical model consisting of a liquid layer in a constant acceleration field acting outwards from the liquid cannot explain the observed instability for all wave numbers above k_c. He suggested that the instability is due to resonances between waves in the liquid layer and the oscillatory component of acceleration. The effect of this oscillatory component of deceleration on the liquid layer stability is discussed in the next section.

Stability Analysis

In what follows, the effect of this deceleration on the stability of a two-dimensional liquid layer of depth h is investigated. The liquid is assumed to be inviscid and initially quiescent so that its subsequent motion can be represented by a potential function. Moreover, the effects of the external gas are neglected. A Cartesian x-y coordinate system is employed with the x axis in the plane of the undisturbed surface, and the y axis normal to this surface. If the surface is disturbed, then the potential function $\phi(x,y,t)$ representing the motion due to this disturbance satisfies the equation

$$\nabla^2\phi = 0 \text{ for } -\infty < x < \infty \text{ and } -h \leq y \leq \eta \tag{2}$$

where $\eta(x,t)$ is the surface disturbance. The normal velocity at the body vanishes, and hence

$$\phi_y(x, -h,t) = 0 \tag{3}$$

At the free surface, the boundary conditions, assuming infinitesimal disturbances, are

$$\phi_y = \eta_t \quad \text{on} \quad y = 0 \tag{4}$$

$$\rho\, g(t)\eta - \rho\,\phi_t + T\eta_{xx} = 0 \quad \text{on} \quad y = 0 \tag{5}$$

where

$$g(t) = g_0 + g_a \cos 2\omega t \tag{6}$$

Since the system is linear, the initial conditions are taken to be

$$\eta(x,0) = \eta_0 \cos kx \tag{7}$$

$$\eta_t(x,0) = 0 \tag{8}$$

It can be shown that the solution of Eqs. (2–8) is

$$\eta(x,t) = \eta_0\, u(t) \cos kx \tag{9}$$

$$\phi(x,y,t) = \eta_0\, v(t) \cosh k(y + h) \cos kx \tag{10}$$

where

$$v = \dot{u}/k \sinh kh \tag{11}$$

$$\ddot{u} + [Tk^2/\rho - g(t)]k \tanh khu = 0 \tag{12}$$

Letting $\tau = \omega t$ in Eq. (12) and using Eq. (6) gives

$$d^2u/d\tau^2 + [\mu - 2\gamma \cos 2\tau]u = 0 \tag{13}$$

where

$$\mu = \frac{(Tk^2/\rho - g_0)k \tanh kh}{\omega^2}, \quad \gamma = \frac{g_a k \tanh kh}{2\omega^2} \tag{14}$$

Equation (13) is the well-known Mathieu equation[8] with stable or unstable solutions depending on the parameters μ and γ. In the stable case, the solutions are either periodic or almost periodic. In the unstable case, on the other hand,

Received March 24, 1969; revision received June 2, 1969.

* Manager, Mathematical Physics Department. Member AIAA.